Asian Journal of Chemistry; Vol. 29, No. 5 (2017), 1161-1167
ASIAN JOURNAL OF CHEMISTRY
https://doi.org/10.14233/ajchem.2017.20495

Dealloying of Cu-Ag Alloys in Sodium Sulphate Solutions

MISHAEL A. AL-KHALDI[1], AYMAN M. ZAKY[1,2,*] and NADA K.M. AL-EIDAN[1]

[1]Chemistry Department, College of Sciences, Dammam University, P.O. Box 1982, Dammam 31441, Saudi Arabia
[2]Chemistry Department, Faculty of Sciences, South Valley University, Qena 83523, Egypt

*Corresponding author: E-mail: azaky1@yahoo.com

Received: 5 January 2017; *Accepted*: 31 January 2017; *Published online*: 10 March 2017; AJC-18319

The electrochemical behaviour of copper-silver system was studied in 0.1 M Na_2SO_4 using cyclic voltammetry, potentiodynamic anodic polarization and current-time transients techniques are used to study the electrochemical behaviour of copper-silver alloys was studied in 0.1 M Na_2SO_4. Microstructure characterization and surface morphology of the compounds formed on the electrodes surfaces during electrochemical processes are carried out using XRD and SEM and EDX analysis. The anodic portion of the voltammogram was characterized by the existence of two potential regions I and II separated by certain critical potential, E_{crit}. In 1st potential region preferential dissolution of copper occurs and leads to the appearance of three anodic peaks A_1, A_2 and A_3 which are related to the formation of soluble Cu^+ species, Cu_2O and [CuO-$Cu(OH)_2$], respectively. As soon as the critical potential, E_{crit}, was reached the current density raises sharply indicating surface enlargement and the onset of region II where copper and silver dissolve simultaneously. The preferential dissolution of copper was enhanced and the critical potential was decreased on increasing the silver content in the alloy. Potentiostatic current/time transients showed that the formation of Cu_2O, CuO and $Cu(OH)_2$ layers involves a nucleation and growth mechanism under diffusion control.

Keywords: Copper-silver alloys, Surface enlargement, Cyclic voltammetric, Current/time transients.

INTRODUCTION

Due to the highly electrical and thermal conductivity of coatings consist of copper-silver alloys; it is used in low power circuits in electronics [1] in comparison to coatings of pure copper or pure silver. Alloying silver with copper conserves silver and reduces costs [1]. In cyanide and acid solutions, the dissolution of silver, copper and silver-copper alloys was studied where ferric ion or oxygen is added as an oxidant [2], in sulfuric acid [3] or in aerated ammonical solution [4,5]. Various electrochemical perpetuations as cyclic voltammetric, potentiodynamic anodic polarization and current-time transients are used to study copper-silver alloys electrochemically in sodium carbonate [6], in sodium carbonate containing chloride ion [7], in sodium hydroxide [8] and in sodium hydroxide containing sulphide ions [9] and perchlorate ions [10]. It was found that the galvanic coupling effect decreased the dissolution of silver, more noble constituent and increased the dissolution of copper, the less noble constituent.

EXPERIMENTAL

Pure copper (99.99 %), pure silver (99.99 %) and three copper-silver alloys are used in studying the voltammetric behaviour of Cu-Ag alloys in Na_2SO_4 solution. The alloys were made by fusion of pure two metals in a graphite crucible at a desired temperature in the Research Laboratory of the Aluminum Company of Egypt, cooled and rub off into the suitable cross sectional area. The specimens were inserted into a Teflon mount to get only a cross sectional areas are in contact with solution. The electrodes are polished with emery papers, degreased with acetone then rinsed with doubly distilled water and transferred electrochemical cell. The composition of the studied alloys are described in Table-1. All solutions used in the present investigation were prepared from AnalaR grade chemicals and used without further purification. All the solutions and reagents employed were freshly prepared using doubly distilled water. A 100 mL capacity electrochemical cell was used in this investigation. The electrochemical cell consists of three compartments where two of them are used for the counter and the working electrodes. The reference electrode is inserted in the third compartment. The reference electrode is saturated calomel electrode (SCE). Graphite specimen with large surface area is used as counter electrode. Before each run the cell was washed with first and second distilled water, filled with the test solution and then kept in air thermostat to attain the required temperature ± 0.5 °C. The cyclic voltammetric behaviour of metals and alloys was studied using solutions under consideration and under different experimental

TABLE-1
COMPOSITION OF THE STUDIED ALLOYS

No.	Type	Name	Composition (%)	
			Cu	Ag
1	Cu-Ag	Alloy-1	80	20
2	Cu-Ag	Alloy-2	50	50
3	Cu-Ag	Alloy-3	20	80

conditions. In this set of experiments, the cyclic voltammetric perturbation was applied by means of Gamry potentiostate Interface100 (Potentiostat/Galvanostst/ZRA) operated with IBM compatible PC computer and corrosion software Echem Analyst (version 6.25).

Cyclic voltammetric behaviour of copper-silver alloys were studied under the influence of alloy composition, scan rate (v, mV s^{-1}), reversal potential and number of repeated cycles. Most of the experiments were duplicated and the reproducibility for this type of measurements was found to be satisfactory. The surface of the alloys during electrochemical behaviour measurements was examined for their surface morphology and the kind of compounds formed at particular potentials. The surface morphology of the metals and alloys was studied using scanning electron microscopy (SEM) in ESEM and EDS characterization, Research and Development Center, Advanced Analysis Unit in Aramco company, model FEI QUANTA 400 F. ESEM was operated at voltage up to 30 kV and magnification power up to 200000 times. The microstructure of the compounds formed on the electrode surface was obtained using x-ray diffraction analysis using (PANalytical X'Pert PRO) diffractometers. This equipment is located in, Research and Development Center, Advanced Analysis Unit in Aramco company, A manual search and match is carried out using JCPDS powder diffraction for compound identification.

RESULTS AND DISCUSSION

The electrochemical behaviour of pure copper, (Fig. 1 curve 1) was studied between E_c = -1600 mV and E_a = 200 mV in 0.1 M Na_2SO_4 solution at 25 °C and scan rate dE/dt = 50 mV s^{-1} and was characterized by the appearance of three anodic peaks A_1, A_2 and A_3. The anodic peaks A_1 was related to the formation of soluble Cu^+ ions [11,12]. The anodic peaks A_2 and A_3 are related to the formation of Cu_2O [13,14] and CuO-$Cu(OH)_2$, respectively [11,15].

$$2Cu + H_2O \longrightarrow Cu_2O + 2H^+ + 2e^- \quad A_2 \quad (1)$$

$$Cu_2O + H_2O \longrightarrow CuO + 2H^+ + 2e^- \quad A_3 \quad (2)$$

$$Cu_2O + H_2O \longrightarrow Cu(OH)_2 + 2e^- \quad A_3 \quad (3)$$

At potential value more than that of the anodic peak A_3 involves Cu pitting as the main process yielding Cu^{2+} species [16]. The reverse scan exhibited the appearance of hysteresis loop of pitting corrosion [16]. At the same time, it appears the existence of the four cathodic peaks C_1 C_2, C_3 and C_4. The cathodic peak C_4 is attributed to the electrodeposition of soluble Cu^{2+} to Cu [16]. The cathodic peaks C_3, C_2 and C_1 are ascribed to the reduction of CuO-$Cu(OH)_2$ to Cu_2O, Cu_2O to Cu and soluble Cu^+ to Cu, respectively [16].

Typical cyclic voltammograms of pure silver (Fig. 1, curve 2), was studied between E_c = -1600 mV and E_a = 400 mV in

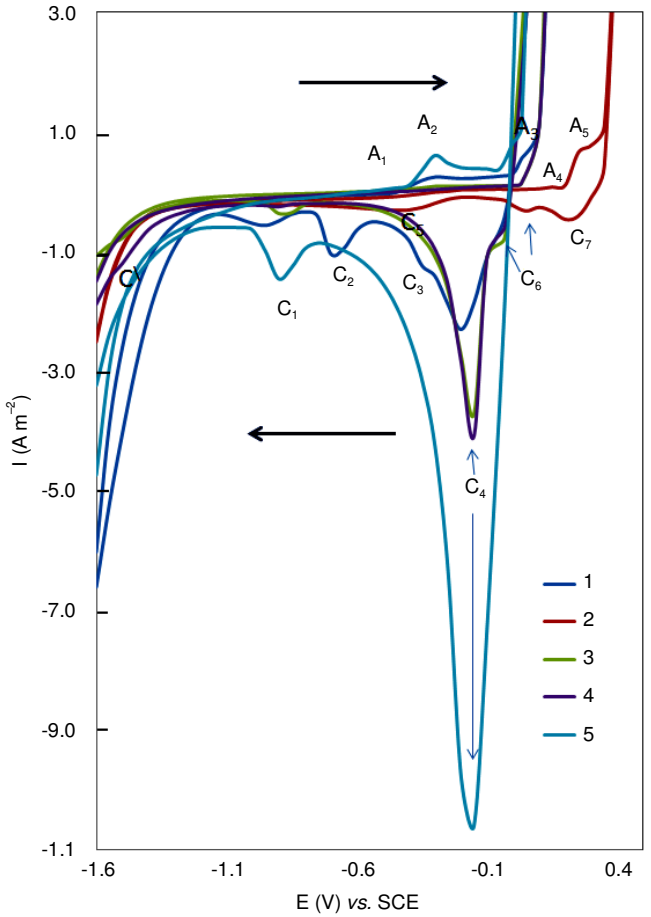

Fig. 1. Cyclic voltammograms of (1) copper, (2) silver, (3) alloy3, (4) alloy-2 and (5) alloy-1 in 0.1 M Na_2SO_4 at 25 °C and scan rate 50 mV s^{-1}

0.1 M Na_2SO_4 solution at 25 °C and scan rate dE/dt = 50 mV s^{-1}. However the general shape of the voltammogram is typical of the voltammogram obtained by previous worker [17]. Two anodic (oxidation) peaks A_4 and A_5 are observed prior to oxygen evolution reaction. Three cathodic peaks C_5, C_6 and C_7 are observed on sweeping the potential in the negative direction. These results indicated that the anodic peak A_4 is in conjugation with the cathodic peak C_5 and the anodic peak A_5 is in conjugation with the cathodic peak C_6. In general the anodic peaks A_4 and A_5 are due to the dissolution of silver to form Ag_2O and AgO [17] which indicates that in neutral solution dissolution should takes place at potential which is more active than that for the formation of the lowest oxide.

$$Ag + H_2O \longrightarrow Ag_2O + 2H^+ + 2e \quad A_4 \quad (5)$$

$$2Ag_2O + H_2O \longrightarrow Ag_2O_2 + 2H^+ + 2e \quad A_5 \quad (6)$$

The cathodic peaks C_5, C_6 and C_7 are ascribed to the reduction of Ag_2O to Ag, Ag_2O_2 to Ag_2O and Ag_2SO_4 to Ag, respectively [17].

Fig. 1, curves 3, 4 and 5 show the cyclic voltammograms of the three alloys in 0.1 M Na_2SO_4, at scan rate 50 mV s^{-1} at 25 °C. The cyclic voltammograms of copper and silver are superimposed for comparison. On the anodic direction, the voltammograms were swept from -1600 mV (SCE) to more positive potential. On the positive going the current density decreases gradually till reaches zero value (SCE) and then reverses its sign. The anodic sweep of the alloys is charac-

terized by the appearance of three anodic peaks prior to oxygen evolution reaction.

The anodic sweep of the alloys is characterized by two well-defined potential regions prior the onset of surface enlargement at the critical potential $E_{crit.}$:

Region I: Dissolution of copper: This region is characterized by the existence of three anodic peaks A_1, A_2 and A_3 where copper dissolution from the alloy is close to that occurs from pure copper. The anodic peaks A_1 was related to the formation of soluble Cu^+ ions [11,12]. The anodic peaks A_2 and A_3 are related to the formation of Cu_2O [13,14] and CuO-$Cu(OH)_2$, respectively [11,15].

$$2Cu_x\text{-}Ag_y + H_2O \longrightarrow Cu_2O + Cu_{x-2}\text{-}Ag_y + 2H^+ + 2e^- \quad A_2 \quad (7)$$

$$Cu_2O + H_2O \longrightarrow CuO + 2H^+ + 2e^- \quad A_3 \quad (8)$$

$$Cu_2O + H_2O \longrightarrow Cu(OH)_2 + 2H^+ + 2e^- \quad A_3 \quad (9)$$

The peak current density (i_p) of the anodic peaks A_1, A_2 and A_3 of alloys is higher than that of pure copper and increases as the silver content is increased in the alloy due to the galvanic effect [18-20] which enhances the dissolution of copper from the alloy. This galvanic effect leads to shift the potential of these three anodic peaks to more cathodic values [21].

Region II: Dissolution of copper and silver: The voltammograms of the alloys in this region shows a sudden increase in the current to high value indicating the onset of surface enlargement at the critical potential ($E_{crit.}$) followed be the appearance of hysteresis loop in the reverse scan. Fig. 2 shows SEM micrograph that represents the existence of some pits on alloy 3 surface after anodic polarization to 200 mV in 0.1 M Na_2SO_4. It seems that the numerous of pits exists in copper rich phase (dark regions) compared to less number of pits in silver rich phase (white regions) [22]. The critical potential ($E_{crit.}$) is shifted to more active values as the silver content is increased in the alloys as expected from the galvanic couple effect.

X-ray diffraction analysis for the layer formed on the surface of alloy-1 anodically polarized potentiostatically at -100 mV (Fig. 3) showed the existence of Cu_2O, CuO, $Cu(OH)_2$. Potentiostatic polarization of alloy 3 at 200 mV, beyond the critical potential, $E_{crit.}$, (Fig. 4) resulted in the appearance of minor amounts of Cu_2O, CuO, $Cu(OH)_2$, Ag_2O and AgO as can be expected due to destruction of passive films with surface enlargement and the simultaneous dissolution of the two constituents, copper and silver.

Fig. 5 for alloy-1 shows the voltammograms in 0.1 M Na_2SO_4 at 25 °C, 10 mV s^{-1} and different reversing anodic potentials. Reversing the potential at value situated between the potential of the anodic peaks A_1 and A_2 results in the formation of only one cathodic peak C_1. On reversing the potential at value more anodic of the potential of the anodic peak A_2 results in the appearance of the cathodic peak C_2. However a new cathodic peak C_3 appears on reversing the potential at value more anodic to the potential of the peak A_3. The peak current density (i_p) increases and the peak potential (E_p) is shifted to more cathodic potential on increasing the reversal potential value. These results suggest that the anodic peaks A_1, A_2 and A_3 are in conjugation to the cathodic peaks C_1, C_2 and C_3 which are correspond to the reduction of soluble Cu^+

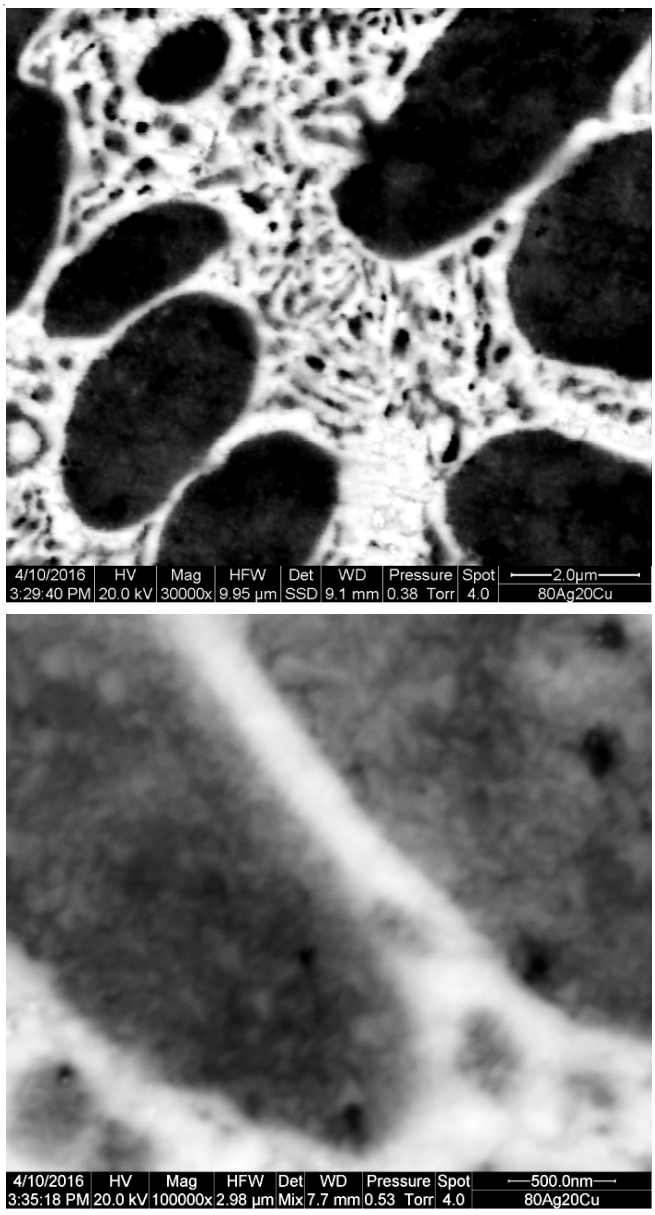

Fig. 2. SEM micrographs of alloy-1 surface in 0.1 M Na_2SO_4 polarized to 200 mV: (upper) x30000 and (lower) x100000

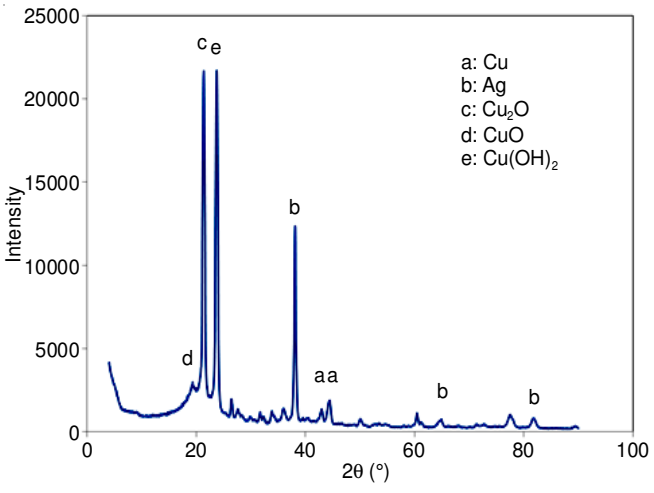

Fig. 3. XRD analysis for alloy-2 polarized to -100 mV in 0.1 M Na_2SO_4 at 25 °C

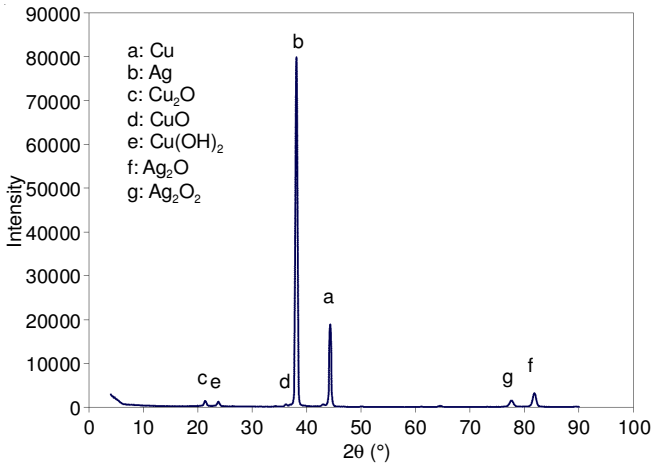

Fig. 4. XRD analysis for alloy-3 polarized to 200 mV in 0.1 M Na_2SO_4 at 25 °C

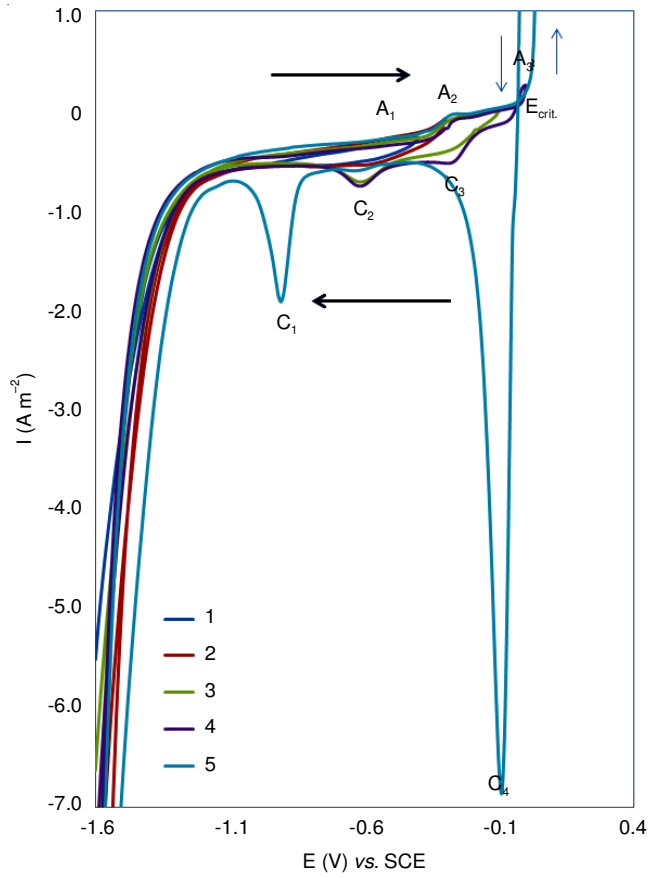

Fig. 5. Cyclic voltammograms of alloy-1 in 0.1 M Na_2SO_4 at 25 °C and different reversing anodic potentials: (1) -420 mV, (2) -330 mV (3) -120 mV (4) -10 mV and (5) 30 mV

to Cu, Cu_2O to Cu, CuO-$Cu(OH)_2$ to Cu_2O. On reversing the potential at value more noble to the critical potential ($E_{crit.}$) the cathodic peak C_4 is appeared as a result of the reduction of $Cu(OH)_2$ and surface enlargement products, Cu^{2+} to Cu^+ and Ag^+ to Ag. The current density of the cathodic peak C_1 is increased as the reversal potential made more noble to the critical potential. The appearance of the cathodic peak C_1 is due to the onset of hydrogen evolution reaction [17].

The effect of sweep rate (dE/dt), ν on the shape of the voltammograms of alloy-1 and alloy-3 was studied by scanning the potential between -1600 mV and nobler potentials in 0.1 M Na_2SO_4 at 25 °C and different scan rate (10-70 mV s^{-1}) and the results are presented in Figs. 6 and 7, respectively. The typical shape of the voltammograms does not affected markedly by changing the scan rate. However the peak current density of the anodic peaks as well as the cathodic peaks is increased by increasing the sweep rate between 10 and 75 mV s^{-1}. The peak potential of the anodic peaks $E_p(A)$ is shifted to more cathodic potential values. The peak potential of the cathodic peaks $E_p(C)$ is shifted to more cathodic potential values with the increase in the sweep rate. The plot of the peak current density of the anodic peaks A_1, A_2 and A_3 of the alloy-1 (Fig. 8) and alloy-3 (Fig. 9) with the square root of the scan rate do not gave a linear straight. These results imply that the processes involved in the appearance of the anodic peaks A_1, A_2 and A_3 are under diffusion control. Similarly, plot of the peak current density of the cathodic peaks C_1, C_4 for alloy-1 (Fig. 10) and of C_1, C_3 and C_4 for alloy-3, (Fig. 11), gave straight lines with the square of the scan rate which implies that the processes involved in the appearance of these cathodic peaks are activation controlled.

Potentiostatic current-time transients are used to examine the electrochemical behaviour of Cu-Ag alloys in 0.1 M Na_2SO_4 solution at 25 °C, were applied for alloy-3 at various anodic potentials E_s and the data is presented in Fig. 12. The current transient densities decrease monotonically with time until reaches a steady state value. The values of the instantaneous and steady state current increase as the step

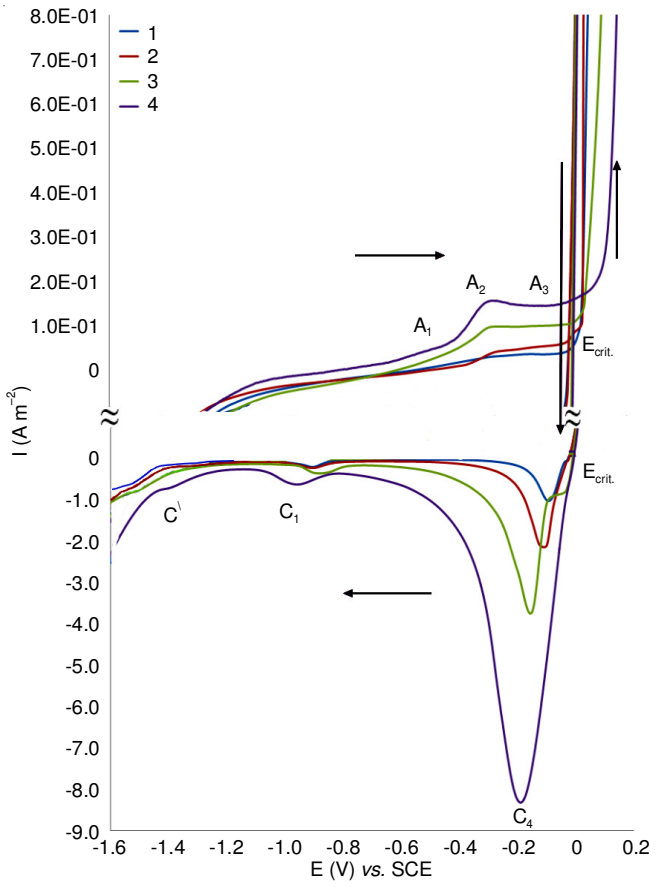

Fig. 6. Cyclic voltammograms of alloy-1 in 0.1 M Na_2SO_4 at 25 °C and different scan rates; (1) 10 mV s^{-1}, (2) 25 mV s^{-1}, (3) 50 mV s^{-1} and (6) 75 mV s^{-1}

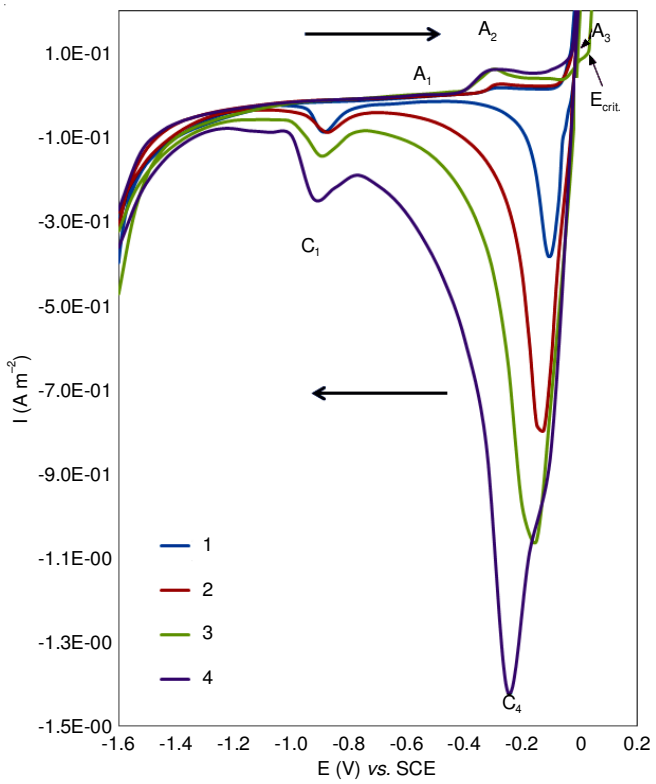

Fig. 7. Cyclic voltammograms of alloy-3 in 0.1 M Na_2SO_4 at 25 °C and different scan rates; (1) 10 mV s^{-1}, (2) 25 mV s^{-1}, (3) 50 mV s^{-1} and (6) 75 mV s^{-1}

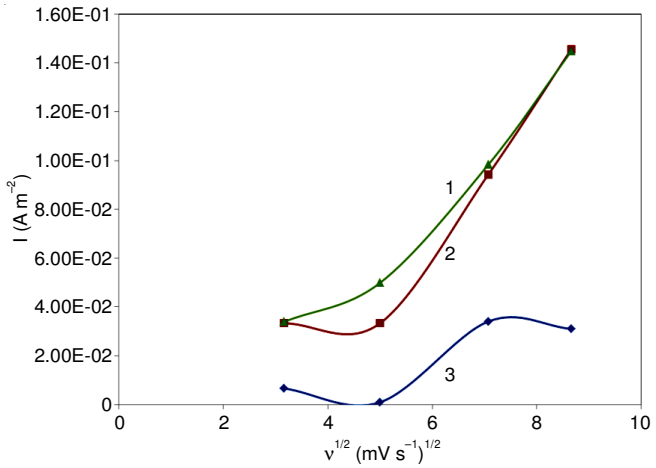

Fig. 8. Relation between of the peak current density i_p of (1) peak A_3, (2) Peak A_2 and (2) peak A_1 on square root of scan rate for alloy1 in 0.1 M Na_2SO_4 at 25 °C

potential is made more positive indicating an increase in the thickness of the anodically formed layers. Plotting the current i *vs.* $t^{-1/2}$ for the continuously decreasing parts of the current transients gives straight lines passing through the origin and gives different distinguishing features (Fig. 13). When E_s is at the potential range of peak A_2, there is only one straight line passing by the origin due to the formation of Cu_2O layer. For $E_s = E_p$ of A_3, the plot consists of three portions with each one obeying a linear relationship. The data are consistent with the formation of three anodic layers Cu_2O and CuO and $Cu(OH)_2$ with three different potential regions. These results indicate that the formation of Cu_2O, CuO and $Cu(OH)_2$ are under diffusion control according to the following equation:

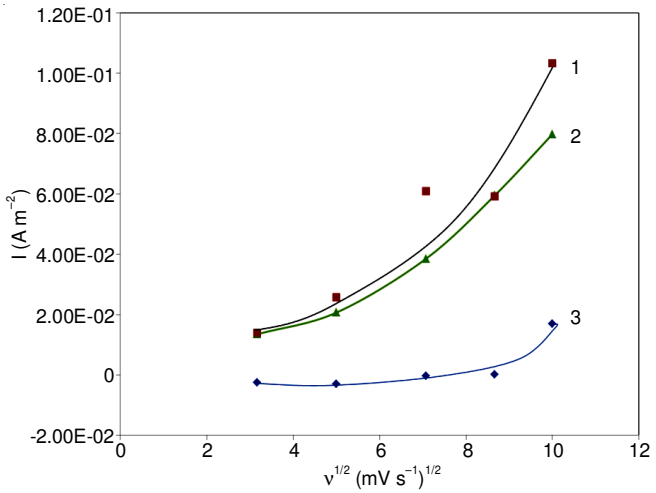

Fig. 9. Relation between the peak current density i_p of (1) Peak A_2, (2) peak A_3 and (3) peak A_1 on square root of scan rate for alloy-3 in 0.1 M Na_2SO_4 at 25 °C

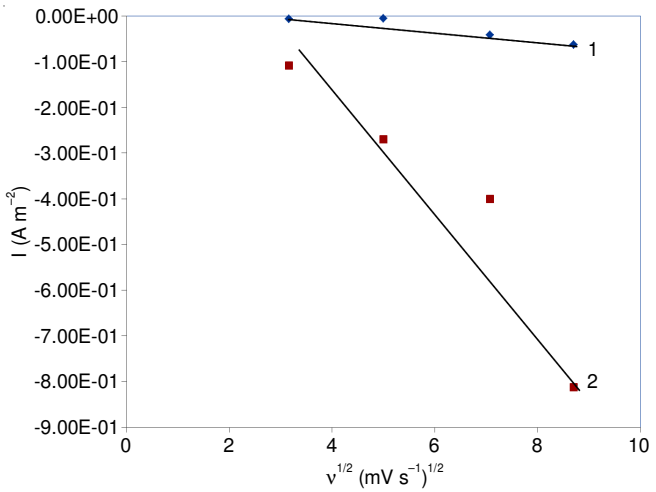

Fig. 10. Linear dependence of the peak current density i_p of (1) peak C_1 and (2) peak C_4 on square root of scan rate for alloy1 in 0.1 M Na_2SO_4 at 25 °C

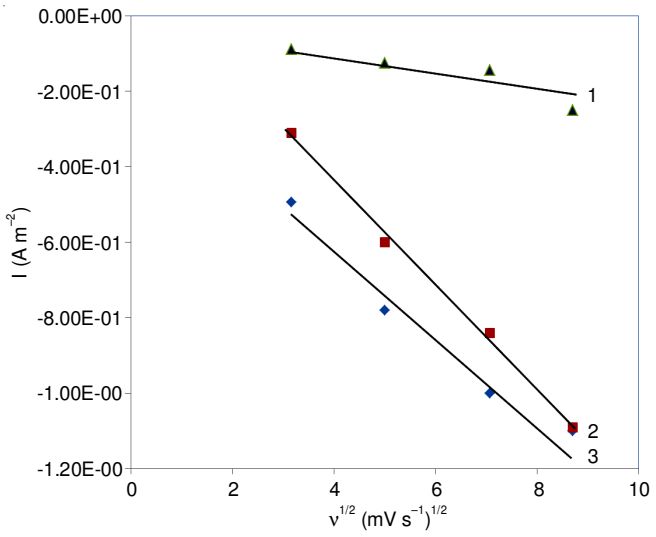

Fig. 11. Linear dependence of the peak current density i_p of (1) peak C_1, (2) peak C_4 and (3) peak C_3 on square root of scan rate for alloy-3 in 0.1 M Na_2SO_4 at 25 °C

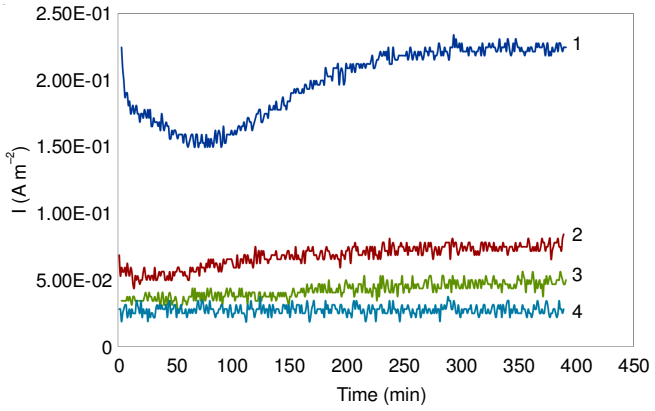

Fig. 12. Current transients at constant anodic step potential E_s for a alloy 3 in 0.1 Na_2SO_4 at 25 °C recorded at: (1) 100 mV, (2) 0.0 mV, (3) -100 mV, (4) -200 mV and (5) -300 mV

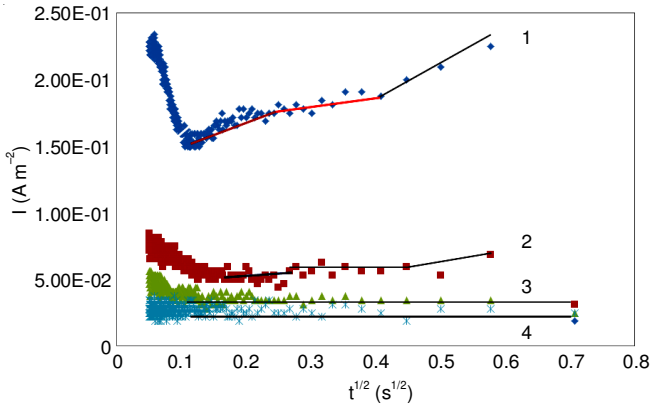

Fig. 13. Dependence of the current density *vs.* $t^{-1/2}$ for descending portions of the current transients for an alloy 3 in 0.1 Na_2SO_4 at 25 °C recorded at: (1) 100 mV, (2) 0.0 mV, (3) -100 mV, (4) -200 mV and (5) -300 mV

$$i = nF\left(\frac{D}{\pi}\right)^{1/2}\frac{C^o - C^s}{t^{1/2}} \quad (10)$$

where C^o and C^s are the bulk and the electrode surface concentrations of the diffusive species and D is the diffusion coefficient of the diffusive species. These results suggest that the formation of Cu_2O, CuO and $Cu(OH)_2$ involve nucleation and growth mechanisms under diffusion control.

Successive CV in the quiescent 0.1 M Na_2SO_4 at 25 °C and scan rate of 20 mV s^{-1} between -1600 and 400 mV for alloy-3 is represented in Fig. 14. Repetitive cycling has a significant effect on the value of the critical potential of the alloy, E_{crit}. As the number of cycle is increased the critical potentials is sifted to more active values. It is seen that, the peak current densities of all anodic peak and all the cathodic peaks is enhanced with the number of repeated cycles. Also, repeated cycling shifts the peak potential of the anodic peaks to more active direction and that of the cathodic peaks to more noble direction. This behaviour is due to an activation of the electrode processes by cycling polarization.

Conclusions

• Cyclic voltammetric behaviour of copper-silver alloys were recorded under the effect of different variables as alloy composition, reversal anodic potentials, scan rate and number of repeated cycles.

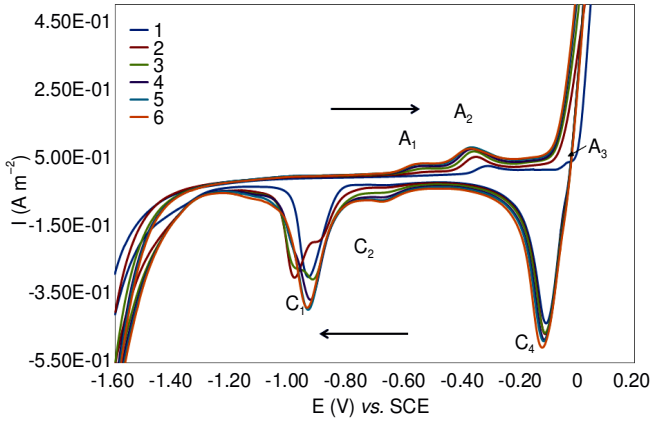

Fig. 14. Cyclic voltammograms of alloy-3 at 25 °C and scan rate 25 mV s^{-1} in 0.1 M of Na_2SO_4 and different repeated cycles; (1) cycle 1, (2) cycle 2, (3) cycle 3, (4) cycle 4, (3) cycle 5 and (5) cycle 6

• The forward (anodic) sweep of the voltammograms is characterized by the appearance of two, selective and simultaneous, potential regions separated by certain critical potential $E_{crit.}$.

• The initial stage of the anodic oxidation of copper-silver alloys involves selective dissolution of the less noble metal, copper component and contains three anodic peaks A_1, A_2, A_3. These peaks are related to the formation of Cu^+ soluble species, Cu_2O, CuO-$Cu(OH)_2$ respectively.

• Increasing the silver content in the alloy enhances the dissolution of copper *via* galvanic coupling effect.

• The backward sweep was characterized by the appearance of four cathodic peaks C_1, C_2, C_3 and C_4. The complementary relationship between the anodic and cathodic current peaks of the alloys was established by stepwise increasing the switching anodic potential E_a stepwise. It was found the cathodic peaks C_1, C_2, C_3 and C_4 are related to the reduction of soluble Cu^+ to Cu, Cu_2O to Cu, CuO-$Cu(OH)_2$ to Cu_2O and surface enlargement products, Cu^{2+} and Ag^+ to Ag, respectively.

• X-ray diffraction analysis at different potentials resulted in different spectra. On polarization to -100 mV showed the existence of Cu_2O, CuO, $Cu(OH)_2$. Potentiostatic polarization to 200 mV resulted in the appearance of minor amounts of Cu_2O, CuO, $Cu(OH)_2$, Ag_2O and AgO.

• The effect of scan rate was studied on the alloys where the dissolution processes in the regions of these anodic peaks was found to be under diffusion control.

• Current – time transients showed the formation of Cu_2O, CuO and $Cu(OH)_2$ involves a nucleation and growth mechanism under diffusion control.

• Repetitive cycling was found to enhance the anodic peaks due to activating the electrode processes by cycling polarization.

• SEM micrograph obtained for alloy-3 surfaces in the vicinity of critical potential ($E_{crit.}$) showed that the electrodes surfaces suffered of pitting attack in the copper rich phase.

ACKNOWLEDGEMENTS

This work was conducted in research units in Dammam University and Saudi ARAMCO, Ad Dammam, Saudi Arabia. This work is a part of thesis of Nada K. Al Edan, Master Student in Chemistry Department, College of Science, Dammam University.

REFERENCES

1. R. Lein and G. Bär, *Elektrie*, **33**, 511 (1979).
2. Y.U. Choi, E.C. Lee and K.N. Han, *Metall. Trans., B, Process Metall.*, **22B**, 755 (1991); https://doi.org/10.1007/BF02651152.
3. L.L. Tokar, T.A. Tarisyna, Y.S. Sorikov, M.S. Igumnov, S.A. Erofeev and C.D. Men'shikov, *Zh. J. Chem.*, **63**, 2638 (1990).
4. Y. Charles and K.N. Han, *Miner. Metall. Process.*, **11**, 12 (1994).
5. Y.C. Guan, *J. Electrochem. Soc.*, **142**, 1819 (1995); https://doi.org/10.1149/1.2044199.
6. A.M. Zaky, *Br. Corros. J.*, **36**, 59 (2001); https://doi.org/10.1179/000705901101501505.
7. A.M. Zaky, *Electrochim. Acta*, **51**, 2057 (2006); https://doi.org/10.1016/j.electacta.2005.07.013.
8. F.H. Assaf, A.M. Zaky and S.S. Abd El Rehim, *Appl. Surf. Sci.*, **187**, 18 (2002); https://doi.org/10.1016/S0169-4332(01)00462-7.
9. A.M. Zaky, S.S. Abd El Rehim and B.M. Mohamed, *Int. J. Electrochem. Sci.*, **1**, 17 (2006).
10. A.M. Zaky and M.A. Al-Khaldi, *Universal J. Chem.*, **1**, 6 (2013).
11. M.R.G. de Chialvo, R.C. Salvarezza, D. Vasquez Moll and A.J. Arvia, *Electrochim. Acta*, **30**, 1501 (1985); https://doi.org/10.1016/0013-4686(85)80012-8.
12. M.R. Gennero De Chialvo, J.O. Zerbino, S.L. Marchiano and A.J. Arvia, *J. Appl. Electrochem.*, **16**, 517 (1986); https://doi.org/10.1007/BF01006847.
13. E. Mattsson, *Electrochim. Acta*, **3**, 279 (1961); https://doi.org/10.1016/0013-4686(61)85004-4.
14. L.H. Jenkins and R.B. Durham, *J. Electrochem. Soc.*, **117**, 768 (1970); https://doi.org/10.1149/1.2407626.
15. R.S. Schrebler, C.H. Gómez and J.I. Gardiazabal, *Corros. Nace*, **43**, 243 (1987); https://doi.org/10.5006/1.3583143.
16. R.M. Souto, S. Gonzalez, R.C. Salvarezza and A.J. Arvia, *Electrochim. Acta*, **39**, 2619 (1994); https://doi.org/10.1016/0013-4686(94)00204-5.
17. B. Abduali, T. Elmira and T. Ainur, *Oriental J. Chem.*, **29**, 33 (2013); https://doi.org/10.13005/ojc/290105.
18. Y.M. Kolotyrkin, *Electrochim. Acta*, **18**, 593 (1973); https://doi.org/10.1016/0013-4686(73)85025-X.
19. W. Machu, A.M. Azzam and G.M. Habashi, *Werkst. Korros.*, **8**, 17 (1957); https://doi.org/10.1002/maco.19570080104.
20. J.A. McMillan, *Chem. Rev.*, **62**, 65 (1962); https://doi.org/10.1021/cr60215a004.
21. J.M. West, Electrodeposition and Corrosion Processes, Nostrand Reinhold, London (1970).
22. M. Hansen and K. Anderko, Constitution of Binary Alloys, McGraw-Hill Book Co., New York, p. 18 (1958).